Materials Science Research International, Vol.9, No.3 pp.187-195 (2003)

Review paper

The High Strain Rate Dynamic Stress-Strain Curve for OFHC Copper

Michael. E. STEVENSON*#, Stanley. E. JONES# and Richard. C. BRADT#
*Metals & Materials Engineers Suwanee, GA 30024, USA
#College of Engineering The University of Alabama
Tuscaloosa, AL 35487-0202, USA

Abstract: The high strain rate ($\sim 10^4$/s) mechanical properties of a 152μm grain size OFHC copper were determined from the analysis of ballistic test specimens subjected to the Taylor Test. Deformation was analyzed by two independent techniques, one an analytical method and the second a finite element numerical model. The results from these complementary analyses were combined to construct a high strain rate dynamic stress-strain curve for this OFHC copper. This dynamic stress-strain curve is then compared with conventional quasi-static mechanical test data. When deformed at these high strain rates, the OFHC copper exhibits an increase in the yield strength, the strain-hardening rate and the ultimate dynamic strength relative to their conventional quasi-static values. The OFHC copper results are then compared with high strain rate measurements for high purity 1100 aluminum. This reveals distinct differences of the high strain rate deformation of these two metals. It is suggested that the differences may relate to the ability of the OFHC copper to deform by twinning, whereas the aluminum does not exhibit a twinning mode of deformation.

Key words: *Aluminum, Copper, Dynamic Stress-strain, Taylor test, Twinning*

1. INTRODUCTION

Dynamic stress-strain responses of materials in the high strain rate regime of $\sim 10^3$-10^5/s and higher are important for many engineering design applications [1–7]. The high strain rate response of a ductile material can be experimentally determined by several experimental techniques. These include ballistic impact tests, such as the one originally developed by Taylor and which bears his name [8]. Although the Taylor Test has tremendous practical significance, there remain challenges relating to the analysis, interpretation and the formal presentation of the results. Analytical models originally advanced by Taylor have experienced considerable refinement since his initial application of the test over a half century ago. However, these models have been mostly one-dimensional and therefore do not always accurately analyze the complex state of stress and strain which is generated during the high velocity impact of the projectile specimen with the non-compliant target. The analytical models appear to be most reliable for the lower strain portions of the deformed Taylor Test specimens.

Recent developments of suitable finite element models for further analysis of the Taylor Test have allowed for considerably greater understanding and an even more extensive analysis of the cylinder impact deformation. However, these models also have their limitations, primarily because the material response during impact does not always ascribe to the familiar theories of quasi-static material response [9, 10]. Another formidable challenge to apply any analysis, or model to Taylor Test specimens are the large gradients of stress, strain and strain rate that occur during the high velocity projectile impact of the ballistic test specimen with the target. It is evident that a more complete analysis of the Taylor Test requires development of a methodology that incorporates the advantages of both analytical and numerical finite element approaches.

This paper reports the development of such a method of analysis and applies it to oxygen free, high conductivity (OFHC) copper. Taylor Test impact specimens of OFHC copper are analyzed by independent analytical and finite element models that provide overlapping results. The two methods of analysis are then combined and utilized to construct a general dynamic stress-strain curve of a universal character. Application of this methodology to express the dynamic stress-strain curve of the projectile specimen allows for a direct graphical representation of the dynamic mechanical response of Taylor Test specimens and depicts the high strain rate response of the test material. In this paper, this combined approach is applied to address the high strain rate deformation of an OFHC copper. It is compared with conventional quasi-static mechanical test data for the same OFHC copper and also with similar high strain rate data for a 1100 aluminum, a pure aluminum.

2. EXPERIMENTAL PROCEDURES

2.1. Specimen Preparation

Specimens of oxygen free, high conductivity copper (OFHC) were prepared to determine both the conventional quasi-static tensile properties and the

Received January 14, 2003
Accepted August 7, 2003

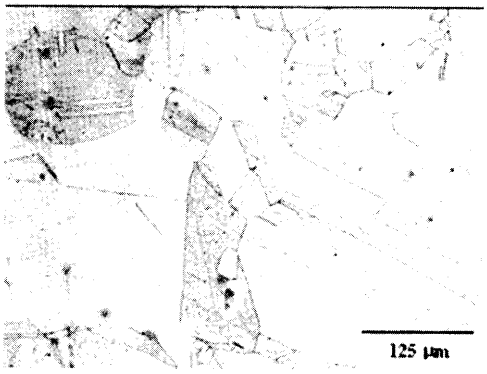

Fig.1. Microstructure of the 152μm average grain size OFHC copper. Note the presence of numerous annealing twins which appear as lines within the grains.

high strain rate dynamic strength-related properties of OFHC copper. A billet of the as-received OFHC copper was mechanically rolled into plate to a final reduction in thickness of 64% using a laboratory scale Stanat rolling mill. The rolling was completed without cross rolling or intermediate annealing. To produce a uniform, equiaxed grain size and to reduce the deformation anisotropy of the OFHC copper, a section of the as-rolled slab was then annealed in air for one hour at 700 ℃. This combination of temperature and time was chosen to yield a reasonably large grain size and to achieve a microstructure that exhibits good ductility during high strain rate impact. The resulting microstructure of this OFHC copper is depicted in Fig.1. Test specimens were prepared from this cold worked and fully annealed OFHC copper for both Taylor Test ballistic impact tests and for conventional quasi-static tensile testing as shown in Fig.2. The long axes for both of these types of test specimens were always maintained in the orientation parallel to the rolling direction of the billet slab.

2.2. Taylor Test Procedures

The Taylor Test is a ballistic impact test where the specimen is the projectile. The test stand utilized for this experiment is shown in Fig.3. From left to right, the first section is the gun tube and projectile firing apparatus. In this study, a 17-caliber gun tube and individually prepared 17-caliber Remington® cartridge cases (0.164in/4.16mm) were used to accelerate a cylindrical copper projectile (3.80g) with flat ends. The explosive propellant was commercial Hercules green dot powder, selected to facilitate a fast, clean burn and the rapid acceleration of the test specimen through the smooth bore gun tube. As usual for experimental guns, there was no rifling in the gun tube, so the Taylor Test projectile did not spin or rotate during firing. To contain the propellant behind the projectile specimen, a nylon obdurator was placed between the loaded cartridge and the cylindrical copper projectile. Cartridges were individually loaded to a precalculated powder charge to control the resultant projectile impact velocity, which enables different levels of total specimen strain and strain rate to be achieved during the test.

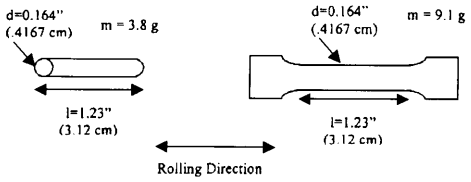

Fig.2. Test specimens for the Taylor Test and conventional mechanical stress-strain testing.

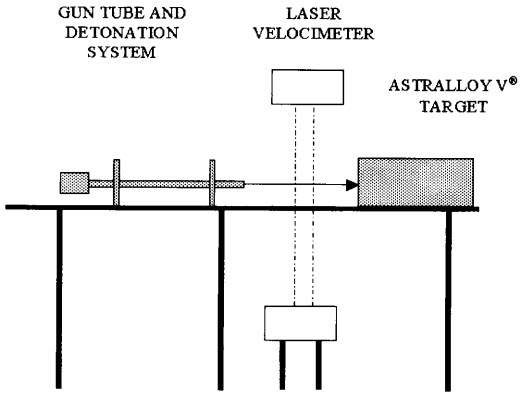

Fig.3. The Taylor Test apparatus.

The projectile specimen velocity measurement system consisted of two parallel laser beams with a photodiode detection circuit coupled to an oscilloscope. A uniform projectile velocity was assumed from the muzzle of the gun tube to the target, a distance of only eight inches or 45.72 cm. Actual velocity measurement was based on the projectile interception of the two parallel laser beams, the length of the projectile and the distance between the two laser beams, 5.08 cm or two inches. This two-beam system and associated electronic circuitry provide a three-fold redundancy of the projectile velocity determination.

The final section of the test equipment is the impact target. It is a 25.4 cm long steel cylinder with a 5.08 cm thick Astralloy V® target face. The target face is attached to the larger steel cylinder with a bolt assembly incorporating a 0.64 cm thick, annealed copper shim plate. It is to insure intimate contact between the target face and the main cylinder as well as a high stiffness upon impact. The target face is designed to separate from the main cylinder to facilitate its hardening and resurfacing (polishing) when dimpling occurs from repeated projectile impacts. The surface of the Astralloy V® target was highly polished to a minor finish with a 0.2-μm diamond paste. Following each individual impact test, the target was rotated slightly to be sure every impact occurred on a

freshly polished surface site.

2.3. Quasi-Static Tensile Testing

Quasi-static tensile testing was performed using a commercial Instron Model 5581 floor mounted, 10,000 lb. universal testing machine to determine the tensile mechanical properties of the OFHC copper. Tensile specimens were pulled at a crosshead speed of 125×10^{-4} in/s (3.175 cm/s). This corresponds to a strain rate of only 1×10^{-4}/s. By contrast, the strain rates achieved during the Taylor Test are on the order of $10^4\sim10^5$/s and higher. Three separate tensile tests were performed at the previously described specimen heat treatment. Yield strengths were determined based on the 0.2% offset method. A typical quasi-static tensile stress-strain curve is presented along with the resulting dynamic stress-strain curve in the discussion.

3. RESULTS AND DISCUSSION

3.1. Characterization of the OFHC Copper Microstructure

Prior to addressing the dynamic mechanical properties of this OFHC copper it is necessary to characterize the microstructure that was produced by the cold working and annealing. Figure 1 depicts the microstructure of the OFHC copper produced through the combined cold work (64% reduction) and recrystallization annealing (700 ℃) heat treatment. In addition to the large, 152±6.2 μm polycrystalline grain size, this OFHC copper microstructure also contains numerous crystallographic annealing twins within the individual grains. These annealing twins appear as straight lines across the grains in the micrograph. Twins are commonly observed in annealed and recrystallized copper. These twins are established to be of the {1 1 1} <1 1 $\bar{2}$> variety and from the crystallographic perspective are identical to the deformation twins which form in copper.

3.2. Taylor Test Results

Figure 4 illustrates several of the deformed Taylor Test impact specimens. At the far left in the photograph is an original, undeformed OFHC copper cylinder for direct comparison. The mushroom shape deformation towards the impact face of the cylinder is evident. Two different approaches were applied to estimate the dynamic state of stress during the deformation of these Taylor Test specimens and also to subsequently develop the dynamic stress-strain-strain rate values. The two technical approaches are then combined to produce a single dynamic stress-strain rate curve for a strain rate of $\sim10^4$/s.

For the initial estimate of the dynamic deformation state, the analytical model of Jones, et al [12] was applied. This approach estimates both the dynamic stress and strain rate of the material for the lower levels of compressive strain in the specimen. It also provides for a comparison with the numerical results

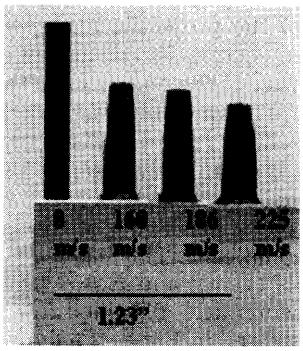

Fig.4. An untested Taylor Test specimen and several specimens after testing.

obtained through subsequent finite element modeling. This uniaxial, one-dimensional model was applied for its refinement beyond the original dynamic stress estimate of Taylor [8]. Furthermore, it is simple in form and easily applied to the deformed specimens such as those illustrated in Fig.4. This elementary dynamic theory estimates both the compressive stress and compressive strain rate for a section of the Taylor Test impact specimen that has undergone compressive strain that is less than, or equal to any specific value that one desires to choose for analysis.

In practice, the above analysis is most satisfactorily applied to the back end, low strain section of the Taylor Test specimen. In this region the dynamic strains and strain rates are less than that of the highly deformed, extensively mushroomed impact end of the test specimen [12] For this particular study, true compressive strain values of 0.1, 0.2, and 0.3 were chosen for the analysis. The dynamic stresses were determined from the following relationship:

$$\sigma_d = \sigma_{qs}(\varepsilon) + \frac{(1+\varepsilon)(1-\beta)^2}{\varepsilon}\rho V_0^2, \qquad (1)$$

where σ_d is the dynamic stress and $\sigma_{qs}(\varepsilon)$ is the quasi-static stress level for the specified strain. The values of $\sigma_{qs}(\varepsilon)$ were obtained from the conventional quasi-static tensile test data. Here ε is the compressive strain, β is a constant related to the impacting projectile deformation, ρ is the density of the projectile test specimen, assumed constant at 8.96g/cc for copper, and V_0 is the projectile impact velocity for the specimen. It should be evident that different impact velocities will produce different levels of dynamic stress, dynamic strain and also different dynamic strain rates.

In addition to the dynamic stress level, the dynamic strain rate at which the aforementioned dynamic stress is achieved during the test must also be determined. The dynamic true compressive strain rate can be estimated from the following equation:

$$\dot{\varepsilon} = \frac{-V_0}{(L_0 - \bar{l})\cdot\exp(\varepsilon)}. \qquad (2)$$

Here $\dot{\varepsilon}$ is the dynamic strain rate and ε is the plastic strain. The projectile impact velocity is V_0, L_0 is the

initial length of the projectile test specimen and $\bar{l}$ is the undeformed section length at the end of the initial transient stage of the plastic wave that is produced during impact. The value of $\bar{l}$ was determined directly from other specimen length measurements through a procedure that is completely described elsewhere [11] . This one-dimensional analysis applies after the initial transient and shock hardening of the specimen material has been completed.

Applying this theory and Eqs.(1)and(2) to the dimensional measurements obtained from the deformed specimens illustrated in Fig.4, the dynamic stress and dynamic strain rate parameters can be estimated for any desired individual strain levels of an impacted Taylor Test specimen. Results for this type of dynamic analysis are illustrated in Fig.5 for the one dimensional analysis incorporating the revised Johnson-Cook model. It is evident that as the strain rate is increased, the dynamic stress level also increases. However, the extent to which the dynamic stress level increases with increasing strain rate is not completely defined by this analytical model alone. It is the reason for complementing the above analytical model with the following finite element analysis.

In addition to the direct analytical description of the dynamic stress-strain which has just been described, a method that is capable of estimating the dynamic state of stress throughout the entire test specimen is desirable. That cannot be accurately achieved through simple analytical modeling, which leaves numerical methods as the most logical approach. For Taylor Test data the popular EPIC (Elastic Plastic Impact Code), combined with a specific strength model, has been demonstrated to be convenient among the possible suitable finite element codes [13,14].

For this analysis, a revised form of the Johnson-Cook (RJC) strength model was employed in combination with the finite element code EPIC. The benefit of this model is that it does not apply any artificial constraints on the strain rate sensitivity of the dynamic stress, which was a weakness of the original Johnson-Cook model [14]. The RJC model has the form:

$$\sigma_d = (C_1 + C_2\varepsilon^N)(1 - T_H^m) \left[1 + C_3 \ln\dot{\varepsilon} C_4 \left(\frac{1}{C_5 - \ln\dot{\varepsilon}} - \frac{1}{C_5}\right)\right]. \quad (3)$$

In Equation(3), σ_d is the dynamic stress, ε is the compressive plastic strain and $\dot{\varepsilon}$ is the dynamic strain rate. The T_H is the specimen material homologous temperature and the C_i, N and M are empirical coefficients that are specifically estimated through an iterative curve fitting process that is contained within the structure of the EPIC code [13].

The same strain measurements that were previously used in the analytical model were incorporated into the EPIC code to determine the constants of Eq.(3). The EPIC coefficients, C_1 and C_2 and N are strength parameters that apply to the stress-strain response of the material. They are independent of the strain rate. The coefficients C_3 to C_6 relate to the strain rate sensitivity of the test specimen. The coefficient M is applied only to those calculations where the initial temperature of the impact test specimen is varied. The constants resulting from the application of the EPIC code to the above equation from the analyses for the 152±6.2 μm grain size OFHC copper are surnmarized in Table 1.

From the empirical coefficients of the RJC model determined by the finite element code, EPIC, the dynamic stress is determined as a function of the strain rate for a specified level of plastic strain. The only constraint which is applied to the strain rate sensitivity is that:

$$\left[1 + C_3 \ln\dot{\varepsilon} + C_4 \left(\frac{1}{C_5 - \ln\dot{\varepsilon}} - \frac{1}{C_5}\right)\right] \leq C_6. \quad (4)$$

Here, C_6 is an empirical constant that limits the maximum dynamic stress that can be achieved for dynamic strain rates beyond a critical value of the strain rate. The critical strain rate, $\dot{\varepsilon}_{crit}$, can be determined directly from the model by applying the following equation:

$$\dot{\varepsilon}_{crit} = e^{C_5} \cdot \sec^{-1}. \quad (5)$$

Utilizing this form of the RJC model, a series of dynamic stress vs. strain rate plots can be generated for the same strain values determined from the analytical model. Curves for 20% strain are shown along with the individual points for the analytical model results in Fig.5.

Similar to the previous results from the analytical model, the numerical results suggest that the dynamic stress increases significantly with increasing strain rate at a strain rate of $\sim 10^4$/s. This type of a rapid increase of dynamic stress with increasing strain rate is similar to that which has been reported by Khan and Huang [15] for 1100 aluminum. The results presented in Fig.5 also illustrate that there is significant strain rate dependence of the dynamic stress.

Table 1. The empirical revised Johnson Cook model for the 152μm average grain size OFHC copper in this study.

Grain Size(μm)	152	C_5	10.020
		C_6	4.720
C_1(MPa)	76.50	N	0.122
C_2	132.90	M	1.048
C_3	0.001	$\dot{\varepsilon}_{crit}$	2.25E+04
C_4	0.189		

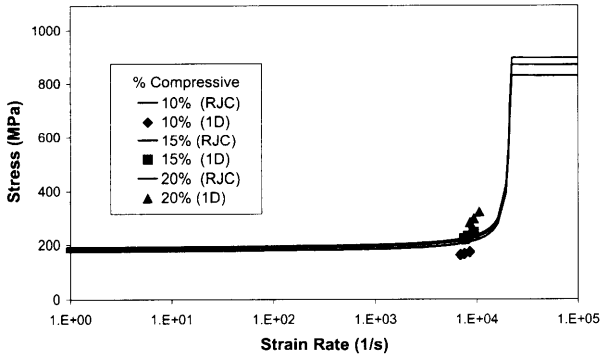

Fig.5. Stress vs strain rate results for the 152μm average grain size OFHC copper with the one dimensional model and from the EPIC numerical analysis.

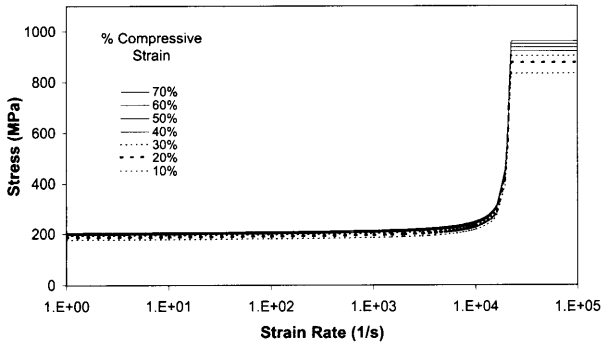

Fig.6. The stress vs strain rate results for the 152μm average grain size OFHC copper at a series of constant strains through application of the RJC strength model and the EPIC code.

However, this analysis does not fully convey the dynamic state of stress for the entire deformed Taylor Test impact specimen. This is important, for it is evident from the actual test specimen geometry in Fig.4 that the Taylor Test specimens have a significant strain gradient from the mushroomed impact face towards the back of the specimen.

The revised Johnson-Cook (RJC) strength model allows for two different presentations of the state of dynamic stress in Taylor Test specimens. One is for the case of constant strain. It is identical to the results presented in Fig.6. It is possible to construct a series of such curves for the different strain levels observed in the highly deformed Taylor Test specimens. Such a series of constant strain curves has been developed for the 152μm average grain size OFHC copper specimens and is shown in Fig.6. This representation of the strain rate dependence of the dynanric stress provides substantial insight to the deformation. However, because of the nature of the logarithmic scale it is difficult to visually ascertain just which stress level occurs at which strain rate for any given measured strain from this type of a series of curves.

Another option to present the dynamic states of stress throughout a single Taylor Test specimen is to

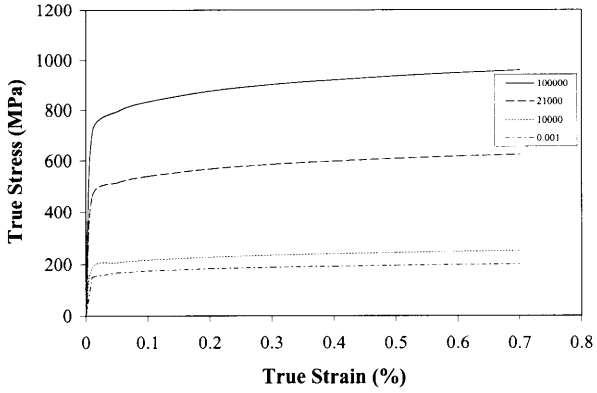

Fig.7. Conventional stress-strain curves for the 152μm average grain size OFHC copper generated from the Taylor Test specimens for a series of different strain rates.

generate of a series of dynamic stress-strain curves, each for a constant strain rate. This alternative form of representation is shown in Fig.7. It is more familiar to most materials scientists and also more direct for an analysis of the strain rate dependence of the dynamic stress-strain curves. Meyers and Chawla [16] present a similar series of stress-strain curves for a 1040 steel, while Sinha, et al [17] present the same type of curves for polycrystalline MgO. However, it is not an optimal presentation of the state of stress for a complete Taylor Test specimen. These analyses illustrate that reliance on the RJC model alone is not a comprehensive means by which the dynamic state of stress can be presented. However, the approach can be utilized in conjunction with the results of the analytical model to construct a specific form of visualization in terms of a general dynamic stress-strain curve.

The results of Fig.5 confirm a critical point that allows for the determination of a more general form of a dynamic stress-strain curve, for there is quite satisfactory, although not perfect, agreement between the analytical and finite element models. This correspondence enables the analytical model to complement the numerical model in a way that the two may be combined. The analytical model estimates the dynamic stress and strain rate for a given strain measurement for a Taylor Test specimen. Its drawback is that its application is restricted to the lowest levels of strain that occur in a Taylor Test specimen. The limiting factor for the numerical model is that both the strain and the corresponding strain rate are both required to determine the dynamic stress.

The numerical model difficulty can be addressed by assuming that the strain rate is proportional to the strain in a Taylor Test specimen. One can then use the strain/strain rate data points obtained from the analytical model to generate a set of strain rate data from the strain measurements obtained directly from the Taylor Test specimens. With this single simple assumption, the analytical and numerical models can

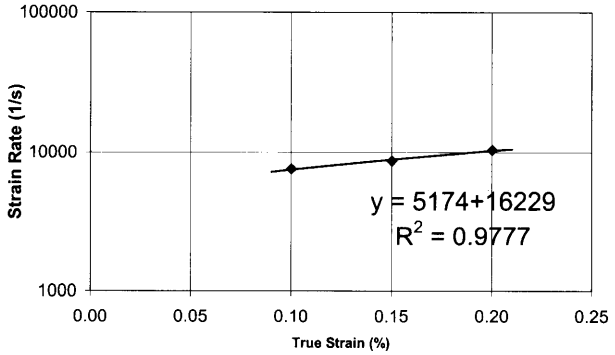

Fig.8. The stress-strain rate relationship for the 22m/s impact velocity Taylor Test specimen of the 152μm average grain size OFHC copper.

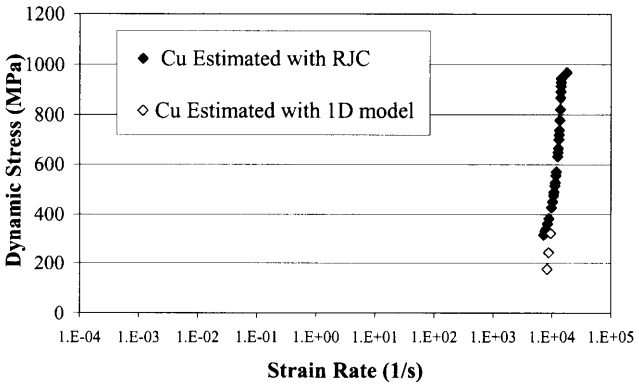

Fig.9. Estimated dynamic stress-strain rate plot for the 152μm average grain size OFHC copper by the two different analysis.

be combined to estimate the state of stress for each strain measurement taken on a Taylor Test specimen. The only assumption is that the strain rate is proportional to the strain in a manner consistent with the results of the analytical model. This is a reasonable assumption, for the entire strain distribution (deformation) of the test specimen occurs over a very short period of time.

Applying a regression analysis to the strain and strain rate data points that are obtained for each Taylor Test specimen, it is possible to linearly relate the strain to the strain rate for that particular test specimen. That form of regression analysis for the 225m/s impact velocity Taylor Test specimen ofthis 152±6.2μm average grain size OFHC copper is shown in Fig.8. The data falls on a straight line, so that to a first approximation, those results can be describcd by the following linear relationship between the strain and the strain rate:

$$\dot{\varepsilon} = A + B\varepsilon. \tag{6}$$

Here A and B are constants that are specific to each individual Taylor Test specimen and must be determined by regression analysis. For the 225m/s impact of 152±6.2μm grain size copper, the intercept A is equal to 16,229/s and the slope B is equal to 5,174/s. From Eq.(6) and these two constants, the dynamic strain rate can then be directly estimated for every strain measurement on the same Taylor Test specimen for which the constants were determined.

Utilizing these strain and strain rate data, the dynamic stress can then be estimated for each set of data points through Eqs.(1)and(2) in conjunction with the eight numerical model constants that were determined for the 152μm average grain size OFHC copper. The results of that analysis are shown in Table 2. The dynamic stress is plotted as a function of the dynamic strain rate in Fig.9, which is similar to Fig.6. However, Fig.9 incorporates the results from the high strain gradient portion of the same 225m/s impact velocity specimen, rather than just an estimate for a single strain value. The stress and strain data summarized in Table 2 can then be plotted in the familiar stress versus strain form to produce the high strain rate dynamic stress-strain curve which is shown Fig.10.

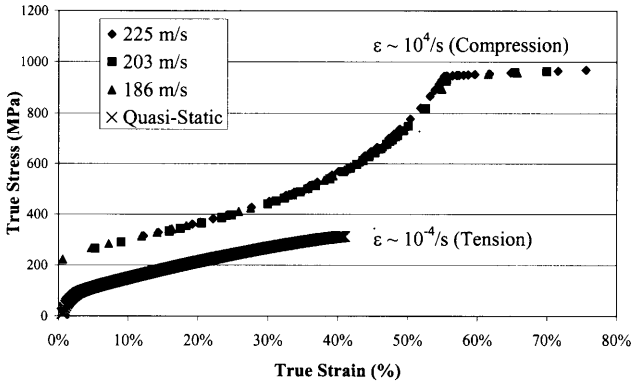

Fig.10. The composite dynamic stress-strain curve 152μm average grain size OFHC copper at a strain rate of $\sim 10^4$/s and the quasi-static σ-ε curve.

The dynamic stress-strain curve in Fig.10 is characteristic of the dynamic stress-strain response of this OFHC copper for a strain rate of $\sim 10^4$/s. This result substantiates the use of the simplifying assumption of a proportional relationship between the strain and strain rate in Eq.(6) and indicates that, at the very least, it serves well as a first approximation. In fact it serves very well as the results for three different test specimens, when separately analyzed, do overlap considerably in Fig.10. This assumption appears to be an excellent approximation for the strain rate gradient in a Taylor Test specimen as it does yield satisfactory results.

In addition to the simplifying assumption previously addressed, the comparison with the quasi-static stress-strain curve generated from a conventional tensile test can also be considered, although it is obvious that the conditions of stress for the test specimens are quite different. A key difference between the dynamic stress-strain curve and a conventional tensile test is that the general dynamic curve represents data that is taken over a range, in fact over a

Table 2. The estimated strain, strain rate and dynamic stress values for a 225m/s Taylor Test specimen of the 152μm average grain size OFHC copper.

ε, %	$\dot{\varepsilon}$, s^{-1}	σ_d, MPa	ε	$\dot{\varepsilon}$	σ_d	ε	$\dot{\varepsilon}$	σ_d
76	17436.6	967	54	14010.9	913	40	11681.4	569
72	16784.4	963	54	13913.9	891	39	11520.0	554
65	15679.5	956	54	13913.9	891	37	11185.0	526
62	15187.3	953	53	13805.0	867	36	11011.1	513
60	14845.5	950	52	13579.9	821	34	10649.7	487
59	14690.3	949	50	13344.6	778	33	10461.9	474
58	14583.7	948	49	13098.5	737	30	10071.2	450
57	14474.6	947	49	13098.5	737	28	9659.1	427
57	14424.9	947	48	12971.2	718	22	8764.6	382
57	14424.9	947	47	12841.1	700	19	8278.5	360
56	14327.0	946	46	12571.4	664	16	7764.0	339
56	14190.1	945	45	12431.8	647	14	7495.2	328
55	14131.1	943	45	12431.8	647	12	7150.1	315
55	14071.4	928	44	12288.8	630			

gradient of strain rates, although it may be a small gradient. Conceptually, this gradient might be visualized in a similar fashion to the "necked" region in a conventional tensile test specimen. Figure 10 illustrates that the dynamic stress stress-strain curve exists at a higher level of stress than the quasi-static stress-strain curve. It is consistent with other observations of an increase of the initial yield strength at high strain rates [9, 15, 16]. Furthermore, for high levels of strain, when the strain rate approaches the critical strain rate, the stress level is limited by the maximum value that results from the application of Eq.(3) This creates a dynamic stress plateau. That plateau consists of all of the RJC plateau stress levels that are calculated for each value of strain. Different yield overlapping results, again justifying earlier assumptions. The dynamic yield stress, dynamic strain hardening rate and the ultimate dynamic stress, as presented in Fig.10, are all considerably greater than the comparable material characterization parameters determined from the conventional quasi-static tensile test.

This is further substantiating evidence for the validity of the dual methodology approach, both analytical and numerical, that the dynamic stress-strain curves which are generated from different velocity Taylor Test specimens produce dynamic stress-strain curves that overlap one another at all values of strain. The physical reason for this overlap is that for identical values of strain from different velocity Taylor Test specimens, the plastic strain rates are also identical. In fact, the entire plastic high strain rate range in a Taylor Test specimen approximately varies from 7.5×10^3/s to 1.5×10^4/s, consistent with the assumption that the strain rate is proportional to the strain.

3.3. Comparison with 1100 Aluminum

It was previously noted that Khan and Huang [15] have completed similar high strain rate studies for 1100 aluminum. From a metallurgical viewpoint, OFHC copper may be considered eomparable to 1100 aluminum. Both metals are nominally pure, both deform easily and both have the face centered cubic, FCC, crystal structure. However, aluminum has a much lower melting point, only 660 ℃ as compared to 1083 ℃ for copper. This suggests that 1100 alurninum may be expected to plastically deform, or flow more easily than the OFHC copper. There is, however, one important plastic deformation difference between these two metals. Copper deforms by dislocation slip and twinning, while aluminum does not exhibit twinning as a deformation mechanism. Deformation twins have never been observed in aluminum to the knowledge of these authors. Basic texts confirm this point [18–21].

The reason for twinning deformation in copper, but not in aluminum, lies in the atomic stacking layer sequence of crystal planes normal to a twin plane. The $\{1\ 1\ 1\}$ $<1\ 1\ \bar{2}>$ twinning plane sequence of layers in the FCC structure constitutes a stacking fault. The stacking fault energy in aluminum is large (low twinning probability) relative to copper, which has a lower stacking fault energy (higher twinning probability). The high stacking fault energy of aluminum reduces its ability to form deformation twins during deformation processes.

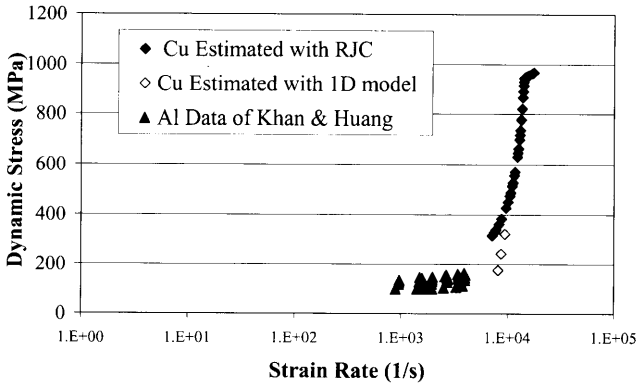

Fig.11. Comparison of the 1100 aluminum from Khan and Huang with the OFHC copper in this study. Note the order of magunitude difference in the strain rates above 10^3/s

Khan and Huang [15] used the direct disc impact experimental technique for measurements and have published results for the high strain rate deformation of the 1100 aluminum. They studied a similar strain rate range as that for the OFHC copper reported in this research. Similar to the OFHC copper, the 1100 aluminum exhibits an extensive low strain rate region of gradual, nearly linear dynamic stress vs. strain rate for strain rates of 10^{-4}/s to 10^2/s. However, the rapid increase of dynamic stress with increasing strain rate is an order of magnitude lower for aluminum.

Figure 11 presents the Khan and Huang [15] high strain rate results for 1100 aluminum and the results of the dynamic stress vs. strain rate for the OFHC copper. The difference is evident even though the Khan and Huang results for 1100 aluminum appear grouped as a cluster of data points because of the different original dynamic stress scale in their publication. Their original data clearly indicates that the 1100 aluminum exhibits a rapid increase in the dynamic stress vs. strain rate at a strain rate of $\sim 2\times10^3$/s. The rapid dynamic stress increase for the OFHC copper, however, occurs at a much higher dynamic strain rate, $\sim3\times10^4$/s, which is an order of magnitude strain rate different, higher than the Khan and Huang [15] aluminum result.

Khan and Huang [15] have not provided a mechanistic description of the 1100 aluminum deformation for this very rapid dynamic stress increase region. They state that "a complete description of all the above phenomena is an extremely difficult, if not impossible task." We are in general agreement with their statement from a purely mechanics perspective. However, from a metallurgical perspective, it is possible to offer a technical explanation for the obvious strain rate difference between the OFHC copper in this study and the 1100 aluminum in the Khan and Huang [15] study.

Because aluminum has a much lower melting point than copper, one anticipates that the 1100 aluminum should deform much more easily than OFHC copper. However, the results presented in Fig.11 are exactly the opposite to the trend which the melting points suggest. The dynamic stress for the 1100 aluminum increases at nearly an order of magnitude lower strain rate than it does for the OFHC copper. The 1100 aluminum is more difficult to plastically deform than the OFHC copper. OFHC copper is easier to deform at the very high strain rates ($\sim10^3$-10^4/s) than 1100 aluminum. While a complete understanding of this difference may not be possible with the limited experimental results to date, it is necessary to begin somewhere whenever a unique experimental observation is made.

Plastic deformation of metals are well known to occur by the two processes of dislocation slip and twinning [18, 19]. Dislocation slip occurs in most metals, but twinning only occurs in some and then only when normal dislocation slip is too difficult for some particular reason. As reviewed by Sinha [20] reasons for twinning may be the complexity of the crystal structure, a low deformation temperature, or a high strain rate, among numerous possibilities. Some metals simply do not twin very easily which can be attributed to a high stacking fault energy of the particular element, such as for aluminum, which has never been reported to deform by twinning. In contrast, copper and some brasses and bronzes are known to exhibit significant amounts of twinning during extensive deformation.

A metallurgical explanation of the difference in the rapid increase for the dynamic stress of OFHC copper in contrast with that for 1100 aluminum is simply that the copper can plastically deform more readily at high strain rates because of its ability to flow by twinning. While the 1100 aluminum is restricted to only conventional dislocation motion for its deformation at high strain rates, the OFHC copper deforms by both conventional dislocation motion and also by deformation twinning. Twinning is well known to be a preferred mechanism of deformation at high strain rates, as well as at other conditions where dislocation motion is not so easy. Reed-Hill and Abasschian [21] note that "Under certain conditions a heavily twinned metal can be more easily deformed then one free of twins." The OFHC copper readily twins and has two possible deformation mechanisms (dislocation slip and twinning) while the 1100 aluminum only has one (dislocation slip)

The high strain rate deformation difference between the two metals. Al and Cu may be explained as follows. Both the copper and the aluminum readily deform by conventional dislocation slip processes a strain rates below $\sim10^2$/s and for dynamic stresses of less than $\sim$100MPa. The FCC crystal structure is a quite ductile one. However, once the dynamic strain rate exceeds $\sim10^3$/s, it becomes more difficult for plastic flow by conventional dislocation slip processes to maintain the necessary dynamic strain. This may be a consequence of work hardening from the increase in dislocation density or it may be simply a fundamental rate effect, but it nevertheless occurs. For 1100 aluminum, the dynamic stress for further

plastic flow increases very rapidly once the strain rate of $\sim 10^3/s$ is exceeded. OFHC copper, however, can deform by twinning as well as conventional dislocation slip. Twinning is actually a more suitable and convenient mechanism for deformation at high strain rates [20]. In fact, twinning is favored over dislocation slip at very high strain rates. Above a strain rate of $\sim 10^3/s$, the 1100 aluminum immediately and rapidly becomes more difficult to deform because it can only deform by dislocation slip. The OFHC copper, on the other hand, can also deform by twinning and thus is able to maintain plastic flow by a combination of dislocation slip and twinning. Therefore, the rapid increase in dynamic stress occurs at $\sim 10^3/s$ for aluminum, but does not occur until a higher strain rate for copper.

4. SUMMARY AND CONCLUSIONS

The high strain rate deformation of an OFHC copper with a $152\mu m$ average grain size was experimentally studied by the Taylor Test, a ballistic impact test. Strain rates in excess of $10^4/s$ were measured. Analysis of the projectile deformation was a combination of overlapping complementary analytical and numerical techniques. It was observed that the high strain rate dynamic stress-strain curve for OFHC copper is extended to higher stress levels than for normal quasi-static tensile tests. The dynamic stresses required for the high strain rate deformation of this OFHC copper are much greater than the quasi-static stresses of normal mechanical testing and the work hardening rate is more rapid as well.

Although mechanical testing data at these strain rates is very limited, results have been published for 1100 aluminum. The OFHC copper measured in this study exhibits greater ease of deformation at higher strain rates than the 1100 aluminum. The aluminum and copper will both deform by normal dislocation motion. However, it is believed that the ability of the copper to deform by extensive twinning in addition to conventional dislocation motion allows it to deform much more readily at high strain rates.

Acknowledgment — The authors are grateful for meaningful technical discussions with M. Barkey, W. Rule, G. Warren and M. Weaver regarding various aspects of the technical content of this research.

REFERENCES

1. E. El-Magd, Computers and Industrial Engineering, **37** (1999)195.
2. P. S. Follansbee, Metallurgical Applications of Shock-Wave and High-Strain-Rate Phenomena, (ed. by L. E. Murr, K. P. Staudhammer and M. A. Meyers): Marcel Dekker, New York, NY(1986)451.
3. U. S. Lindholm, A. Nagy, G. R. Johnson, and J. M. Hoegfelt, Transcations of the ASME, **102**(1980)376.
4. M. A. Meyers, Dynamic Behavior of Materials. John Wiley & Sons, New York, NY(1994).
5. M. A. Meyers, Mechanics and Materials. (ed. by R. W. Armstrong, M. A. Meyers and H. O. Kirchner): John Wiley & Sons, New York, NY(1999)489.
6. L. E. Murr, Materials at High Strain Rates, (ed. by T. Z. Blazynski): Elsevier, London, England(1987)1.
7. M. E. Stevenson, S. E. Jones and R. C. Bradt, Fractography of Glasses and Ceramics IV, (ed. by J. A. Varner and G. D. Quinn): Amer.Cer.Soc., Westerville, OH(2000)473.
8. G. I. Taylor, Proc. Royal Society of London A, **194**(1948)289.
9. R. W. Armstrong, Mechanics and Materials, (ed. by R. W. Armstrong, M. A. Meyers and H. O. Kirchner), John Wiley & Sons, NewYork, NY(1999)363.
10. F. J. Zerilli and R. W. Armostrong, Journal of Applied Physics, **61**(1987)1816.
11. S. E. Jones, J. A. Drinkard, W. K. Rule and L. L. Wilson, International Journal of Impact Engineering, **21**(1998)1.
12. S. E. Jones, P. P. Gillis, J. C. Foster, Jr. and L. L. Wilson, Trans. of the ASME, **113**(1991)228.
13. W. K. Rule, International Journal of Impact Engineering, **19**(1997)797.
14. W. K. Rule and S. E. Jones, International Journal of Impact Engineering, **21**(1998)609.
15. A. S. Khan and S. Huang, International Journal of Plasticity, **8**(1992)397.
16. M. A. Meyers nad K. K. Chawla, Mechanical Behavior of Materials, Prentice-Hall, Upper Saddle River, NJ(1999)127.
17. M. Sinha, D. J. Lloyd and K. Tangri, J. Materials Science, **8**(1973)116.
18. R. W. Hertzberg, Deformation and Fracture Mechanisms of Engineering Materials, J. Wiley & Sons, NewYork, NY(1996)107.
19. Deformation Twinning(ed. by R. E. Reed-Hill, J. P. Hirth and Harry Rogers), Gordon and Breach Science Publishers, NewYork, NY(1963).
20. A. K. Sinha, Physical Metallurgy Handbook, McGraw-Hill, NewYork, NY(2001)4.33.
21. R. E. Reed-Hill and R. Abasschian, Physical Metallurgy Principles, PWS-Kent Publishing, Boston, MA(1992)540.